J Math Chem (2010) 48:38–54
DOI 10.1007/s10910-009-9625-2

ORIGINAL PAPER

Numerical solution of nonlinear singularly perturbed problems on nonuniform meshes by using a non-standard algorithm

Higinio Ramos · J. Vigo-Aguiar · S. Natesan · R. García-Rubio · M. A. Queiruga

Received: 11 August 2009 / Accepted: 29 October 2009 / Published online: 12 November 2009

Abstract In this article, we study the numerical solution of singularly perturbed non-linear autonomous initial-value problems by a non-standard algorithm on layer-resolving nonuniform meshes. Here, we use the piecewise-uniform Shishkin meshes, and two other nonuniform meshes which resolve the difficulties arising from the steep gradient of the solution in the initial layer. The present method is intended for solving the nonlinear problem without linearization and provides third-order convergence results. Linear stability of this method is studied. Numerical experiments are carried out to verify the efficiency and accuracy of the method.

Keywords Singularly perturbed initial-value problems · Non-standard algorithm · Piecewise-uniform Shishkin mesh · Nonuniform meshes

H. Ramos · J. Vigo-Aguiar (✉)
Scientific Computing Group, Universidad de Salamanca, Salamanca, Spain
e-mail: jvigo@usal.es

H. Ramos
e-mail: higra@usal.es

S. Natesan
Department of Mathematics, Indian Institute of Technology, Guwahati 781 039, India
e-mail: natesan@iitg.ernet.in

R. García-Rubio
Department of Applied Mathematics, Universidad de Alicante, Alicante, Spain
e-mail: rgr@usal.es

M. A. Queiruga
Department of Applied Mathematics, Universidad de Salamanca, Salamanca, Spain
e-mail: queirugadios@usal.es

1 Introduction

Singular perturbation problems (SPPs) arise in various branches of applied areas like fluid dynamics, optimal control, chemical reactor theory, etc. Because of the presence of a small parameter multiplying the highest derivative, classical numerical methods fail to yield satisfactory numerical results. Therefore, one has to seek some special methods for the numerical solution of SPPs. More details can be found in the books by Doolan et al. [7] and Miller et al. [14]. Other topics concerning SPPs may be found in [17] or [24], or in the references on these articles.

Experimental and theoretical results show that an adiabatic tubular reactor, in which there is occurring a simple first-order irreversible exothermic chemical reaction, can exhibit multiple stable steady states. The chemical and mathematical models of these processes can be found in the articles of Aris [1], and [3]. The mathematical models of these chemical reactions are differential equations with the highest order derivative multiplied by a small positive parameter.

In particular, consider the nonlinear two-point boundary-value problem arising in chemical reactions:

$$\begin{cases} \varepsilon u''(x) - u'(x) + f(u(x)) = 0, \quad x \in (0,1) \\ u'(0) - \alpha u(0) = 0, \quad u'(1) = 0. \end{cases} \tag{1}$$

Here, the function u represents the dimensionless temperature in the reactor, and ε and α are known constants. The function $f(u)$, which represents the rates of chemical production of the species or the rate of heat generation in the reactor, is the Arrhenius reaction rate given by

$$f(u) = b(c-u)\exp\left(\frac{-k}{1+u}\right).$$

The concentrations of the various chemical species involved in the reaction can be determined in a simple manner from a knowledge of u and the stoichiometric coefficients of the species.

Cohen [4, 5], and O'Malley [18] studied the asymptotic behavior of the solution of the BVP (1). Natesan et al. [15, 16] proposed two numerical schemes for the BVPs (1). Recently, Lovas et al. [12] proposed a parallel numerical method for reaction-diffusion equations arising from chemical reactions.

The BVP (1) can be converted into a system of two first-order ordinary differential equations. Moreover, first-order differential equations are frequently employed for describing the dynamics of chemical reactions [2, 6, 10, 11, 21]. By keeping this in mind, here in this article, we study the numerical solution of the following nonlinear autonomous IVP

$$\begin{cases} \varepsilon\, u'(x) = f(u), \quad x \in \overline{D} = [0,1] \\ u(0) = A, \end{cases} \tag{2}$$

where $0 < \varepsilon \ll 1$ is a small parameter (the viscosity coefficient) and $u,\ f(u) \in \mathbb{R}$. We assume that the IVP in (2) admits a unique solution having an initial layer at $x = 0$. In [7], they have solved the nonlinear IVP (2) by exponentially fitted difference (EFD) schemes after linearizing it by Newton's quasilinearization.

O'Malley [18] has studied the asymptotic behavior of the solution of the IVPs. Numerical schemes for linear IVPs are studied in the book by Doolan et al. [7] by using EFD schemes. Miller derived an optimal uniform difference scheme for singularly perturbed linear IVPs in [13]. Farrell [8] proposed a class of uniformly convergent optimal schemes for linear stiff initial-value problems. To apply these methods to nonlinear problems of the type (2), one has to linearize the problem. Alternately, one can use classical finite difference schemes to linear SPPs on some layer resolving meshes. One can get more insight about the application of Shishkin mesh to linear IVPs in the book [14]. Here, in this article, we directly solve the nonlinear IVP (2) by the non-standard algorithm in [20] using nonuniform meshes.

The main merit of this article is to apply the non-standard algorithm on nonuniform meshes to solve the nonlinear IVP (2). By this way one can integrate numerically the IVP in (2) and resolve the effect of the initial-layer by using it on some nonuniform meshes. In particular, when the right hand side of the ODE (2) is a second degree polynomial, then the IVP is solved exactly without any truncation error, independently of the selected mesh. To highlight the necessity of nonuniform mesh for SPPs of the form (2), we applied this scheme on the uniform mesh and obtained the results. From the numerical results it is evident that the use of nonuniform meshes is essential for numerically solving singularly perturbed IVPs of the form (2).

The paper is organized in the following format: Sect. 2 presents the non-standard algorithm for the IVP (2). The local truncation error and linear stability of the numerical scheme are given in Sect. 3. In Sect. 4 we provide the piecewise-uniform Shishkin mesh, and two other nonuniform meshes. Numerical results are given in Sect. 5 for various examples. The paper ends with some conclusions.

2 The non-standard algorithm (NSA)

Let the mesh points of $\overline{D} = [0, 1]$ be

$$x_0 = 0, \quad x_i = \sum_{k=0}^{i-1} h_k, \quad h_k = x_{k+1} - x_k, \quad x_N = 1, \quad i = 1, 2, \ldots, N-1.$$

Suppose we have solved numerically the problem in (2) up to the mesh point x_n, and assuming the localization hypothesis $u_n = u(x_n)$, we want to obtain an approximate value, u_{n+1}, for the solution at the point $x_{n+1} = x_n + h_n$, that is, $u_{n+1} \simeq u(x_{n+1})$. For this purpose we consider on the interval $[x_n, x_{n+1}]$ the approximation of the IVP

$$\varepsilon\, u' = f(u), \qquad u(x_n) = u_n, \tag{3}$$

by the IVP given by

$$\varepsilon\, z' = f_n + J_n\,(z - u_n) + \frac{1}{2}\, H_n\,(z - u_n)^2\,, \qquad z(x_n) = u_n, \tag{4}$$

where

$$f_n = f(u_n)\,, \qquad J_n = \frac{\partial\, f(u)}{\partial\, u}(u_n)\,, \qquad H_n = \frac{\partial^2\, f(u)}{\partial\, u^2}(u_n), \tag{5}$$

that is, we have approximated on $[x_n, x_{n+1}]$ the function $f(u)$ by its second-order Taylor polynomial constructed at the point $u = u_n$. We can solve the problem in (4) exactly, that is to say, without local truncation error, by using the difference scheme

$$z_{n+1} = \begin{cases} z_n - \dfrac{2\,\tan\left(\dfrac{d\,h_n}{2\,\varepsilon}\right)}{-d + (b + 2\,c\,u_n)\tan\left(\dfrac{d\,h_n}{2\,\varepsilon}\right)}\, f_n\,, & \Delta_n > 0\,, \\ z_n - \dfrac{2\,\tanh\left(\dfrac{d\,h_n}{2\,\varepsilon}\right)}{-d + (b + 2\,c\,u_n)\tanh\left(\dfrac{d\,h_n}{2\,\varepsilon}\right)}\, f_n\,, & \Delta_n < 0\,, \\ z_n - \dfrac{2\,h_n}{-2\,\varepsilon + h_n\,(b + 2\,c\,u_n)}\, f_n\,, & \Delta_n = 0\,, \end{cases} \tag{6}$$

where

$$\begin{aligned} a &= f_n - u_n\, J_n + \frac{1}{2}\, H_n\, u_n^2 \\ b &= J_n - u_n\, H_n \\ c &= \frac{1}{2}\, H_n \\ \Delta_n &= -b^2 + 4\,a\,c \\ d &= \sqrt{|\Delta_n|}\,. \end{aligned}$$

After applying this scheme we will take as approximation for the true solution of (2) at x_{n+1} the value $u_{n+1} = z_{n+1}$. Repeating the procedure along the nodes on the integration interval a discrete solution for the problem in (2) is obtained.

3 Local truncation error and linear stability analysis

We assume that the solution $u(x)$ of (2) is sufficiently smooth. By using Taylor series expansion one can obtain the following local truncation error (see [20])

$$T_{n+1} = \begin{cases} \dfrac{1}{12}\,\rho_0(u(x_n))\,h_n^3 + \mathcal{O}(h_n^4)\,, & \Delta_n = 0\,, \\ \dfrac{1}{24}\,\rho_1(u(x_n))\,h_n^4 + \mathcal{O}(h_n^5)\,, & \Delta_n \neq 0\,, \end{cases}$$

where the terms $\rho_0(u(x))\,,\ \rho_1(u(x))$ have the form

$$\rho_0(u(x)) = \frac{-3\,u''(x)^2 + 2\,u'(x)\,u^{(3)}(x)}{u'(x)}\,,$$

$$\rho_1(u(x)) = \frac{3\,u''(x)^3 - 4\,u'(x)\,u''(x)\,u^{(3)}(x) + u'(x)^2\,u^{(4)}(x)}{u'(x)^2}\,.$$

For the linear stability analysis, consider the following test problem

$$\varepsilon\,u'(x) = \lambda\,u(x)\,, \qquad Re(\lambda) < 0\,.$$

When using complex values the method in (6) simply reads

$$z_{n+1} = \begin{cases} z_n - \dfrac{2\,\tan\left(\dfrac{\sqrt{\Delta_n}\,h_n}{2\,\varepsilon}\right)}{-\sqrt{\Delta_n} + (b + 2\,c\,u_n)\tan\left(\dfrac{\sqrt{\Delta_n}\,h_n}{2\,\varepsilon}\right)}\,f_n\,, & \Delta_n \neq 0\,, \\ z_n - \dfrac{2\,h_n}{-2\,\varepsilon + h_n\,(b + 2\,c\,u_n)}\,f_n\,, & \Delta_n = 0, \end{cases}$$

and after applying the method to the above problem we obtain the difference equation

$$y_{n+1} = \exp(\lambda\,h_n/\varepsilon)\,y_n\,.$$

By setting $z = \lambda\,h_n$ we see that the stability function is given by $R(z) = \exp(z/\varepsilon)$. From this one can easily deduce that the present method is A-stable.

4 Nonuniform meshes

Here, in this section, we present the piecewise-uniform Shishkin mesh and nonuniform mesh of Jain [9]. In order to define the Shishkin mesh, consider the following linear IVP

$$\begin{cases} \varepsilon\, u'(x) + a(x)u(x) = f(x), \quad x \in D = (0,1) \\ u(0) = A, \end{cases} \tag{7}$$

where $a(x)$ and $f(x)$ are sufficiently smooth functions, such that $a(x) \geq \alpha > 0$. Under these assumptions the IVP (7) possesses a unique solution exhibiting an initial layer at $x = 0$ (see [7]).

4.1 Shishkin mesh

First, we provide the Shishkin mesh for the IVP (7). In the initial layer region, one requires a fine grid to obtain better approximation for the numerical solution, and a coarse mesh is enough in the outer region, where the solution behaves smoothly. This can be achieved by the piecewise-uniform Shishkin mesh. Let us denote the grid points by $\overline{D}_\tau^N := \{x_i\}_0^N,\ N \geq 2$.

To obtain the Shishkin mesh, we divide the domain $\overline{D}$ into two subintervals as

$$\overline{D} = [0, \tau) \cup [\tau, 1],$$

for some $\tau \in (0,\ 1/2]$. On the subinterval $[0, \tau)$ a uniform mesh with $N/2$ mesh–intervals are placed, where $[\tau, 1]$ has a uniform mesh with $N/2$ mesh intervals. It is obvious that the mesh is uniform when $\tau = 1/2$, and it is fitted to the problem by choosing τ to be the following function of $N,\ \varepsilon$

$$\tau = \min\left\{\frac{1}{2}, \left(\frac{\varepsilon}{\alpha}\right) \ln N\right\}. \tag{8}$$

4.2 Nonuniform mesh-I

Here, we present the nonuniform mesh given in Jain [9]. Let $0 = x_0 < x_1 < \cdots < x_N = 1$, where $h_k = x_{k+1} - x_k$, $k = 0(1)N - 1$ and $\sigma_k = (h_{k+1}/h_k) > 0$, $k = 0(1)N - 2$. Now, we can express the length of the interval as

$$\begin{aligned} 1 = x_N - x_0 &= (x_N - x_{N-1}) + (x_{N-1} - x_{N-2}) + \cdots + (x_1 - x_0) \\ &= h_{N-1} + h_{N-2} + \cdots + h_0 \\ &= (\sigma_0\sigma_1 \cdots \sigma_{N-2} + \cdots + \sigma_0\sigma_1 + \sigma_0 + 1)h_0. \end{aligned}$$

Thus, we have

$$h_0 = \frac{1}{1 + \sigma_0 + \sigma_0\sigma_1 + \cdots + \sigma_0\sigma_1 \cdots \sigma_{N-2}}.$$

By keeping this as a starting value of the first step length the subsequent step-lengths are given by $h_1 = \sigma_0 h_0,\ h_2 = \sigma_1 h_1,\ h_3 = \sigma_2 h_2,\ \ldots$.

Consider the simplest case when $\sigma_k = \sigma$ (a constant), $k = 0(1)N - 2$, then we obtain

$$h_0 = \frac{1-\sigma}{1-\sigma^N}. \tag{9}$$

The value $\sigma > 1$ gives more number of mesh points close to small values of x, while $\sigma < 1$ produces more number of mesh points near to large values of x.

For the IVP (7), the initial layer is at $x = 0$, and therefore, we choose $\sigma > 1$ which produces more number of mesh points near $x = 0$.

4.3 Nonuniform mesh-II

Nonuniform mesh-II is the proper combination of Shishkin and Jain meshes presented in Sects. 4.1 and 4.2, and it produces better approximate solution for the IVP (2).

More precisely, first we divide the domain $[0, 1]$ into two subdomains as $\overline{D} = [0, \tau) \cup [\tau, 1]$ where τ is the same as in (8). We place $N/2$ points uniformly in the subdomain $[0, \tau)$, and place $N/2$ points nonuniformly in $[\tau, 1]$ by following the idea of the nonuniform mesh-I as given in Sects. 4.2. One can notice that in the Shishkin mesh there is a big deviation between the fine and coarse meshes at the transition point, and by this way we can slowly switch over from fine mesh to coarse mesh at the transition point. Indeed, this idea works very well for the test examples given in the next section.

5 Numerical results

To verify the accuracy and efficiency of the present method, we have applied it to various test problems. The numerical results are presented in terms of maximum pointwise errors in tables. Our main goal is to show the higher-order convergence of the NSA on nonuniform layer-resolving meshes.

We present two existing numerical schemes for singularly perturbed linear IVPs (7), which will be used to compare the numerical results obtained by the NSA. The first one is the well-known Exponentially Fitted Difference Scheme (EFD) on uniform mesh, and the second scheme is the backward Euler scheme (*BE*) on the Shishkin mesh.

5.1 Exponentially fitted difference scheme on uniform mesh

The EFD scheme of Doolan et al. [7] for the linear IVP (7) is given by

$$\begin{cases} \varepsilon\, \sigma_i(\rho_i) \left(\dfrac{U_{i+1} - U_i}{x_{i+1} - x_i} \right) + a(x_i) U_i = f_i, \quad x_i \in \overline{D} \\ U_0 = A, \quad \sigma_i(\rho_i) = \rho_i\, a(x_i)[1 - \exp(-\rho_i\, a(x_i))]^{-1}, \quad \rho_i = (x_{i+1} - x_i)/\varepsilon. \end{cases} \tag{10}$$

The EFD Scheme (10) produces first-order uniformly convergent numerical results for linear IVPs.

5.2 Backward euler (BE) scheme on shishkin mesh

In [14], the authors obtained first-order ε-uniformly convergent numerical solution for the IVP (7) on the piecewise-uniform Shishkin mesh by the following backward Euler scheme

$$\begin{cases} \varepsilon \left(\dfrac{U_i - U_{i-1}}{x_i - x_{i-1}} \right) + a(x_i) U_i = f_i, \quad x_i \in \overline{D} \\ U_0 = A. \end{cases} \tag{11}$$

First, we have to linearize the nonlinear IVP (2), to apply the EFD and the backward Euler (BE) schemes.

This is done by considering for $m \geq 0$ the sequence $\{u^{m+1}(x)\}_{m=0}^{\infty}$ of solutions of the linear problems

$$\begin{cases} \varepsilon\, u_x^{m+1} - f_u(u^m) u^{m+1} = f(u^m) - u^m f_u(u^m), \\ u^{m+1}(0) = A, \end{cases} \tag{12}$$

where u_x denotes du/dx and $f_u = \partial f / \partial u$.

The linearized IVP (12) is of the same form as the linear problem (7). With an initial approximation $u^0(x)$, using the EFD or the BE schemes, one can generate the approximations u_i^m to $u^m(x_i)$ at the mesh points. And there exists an m_0 such that for all $m \geq m_0$, u_i^m is an approximation uniform in ε to $u(x_i)$ (see [7]).

Example 1 Our first example is the following nonlinear IVP

$$\begin{cases} \varepsilon\, u' = \exp(-u), \quad x \in [0, 1] \\ u(0) = 0, \end{cases}$$

whose exact solution is given by

$$u(x) = \log\left(1 + \frac{x}{\varepsilon}\right).$$

For each ε the maximum of the absolute errors on the nodal points in the integration interval is obtained by

$$E_\varepsilon^N = \max_{x_j \in [0,1]} |u(x_j) - u_j|.$$

Further, we have also included in these tables the rate of convergence given by

$$p_\varepsilon^N = \log_2 \left(\frac{E_\varepsilon^N}{E_\varepsilon^{2N}} \right),$$

and the ε-uniform rate of convergence which is defined by

$$p^N = \log_2 \left(\frac{E^N}{E^{2N}} \right).$$

where $E^N = \max_\varepsilon E_\varepsilon^N$ (see [22]).

The maximum pointwise errors obtained by the NSA on uniform meshes and the corresponding rates of convergence are presented in Table 1, which show the necessity of nonuniform meshes for singularly perturbed IVPs. Tables 2, 3 corresponds to the NSA on nonuniform meshes I and II respectively. One can see the third-order convergence from these results.

The maximum pointwise errors obtained by the EFD scheme (10) on uniform meshes are provided in Table 4 and the errors with the *BE* scheme (11) on Shishkin

Table 1 Maximum absolute error E_ε^N and the rate of convergence p_ε^N for Example 1 by NSA on uniform mesh

ε	Number of mesh points N				
	16	32	64	128	256
10^{-2}	$5.2857 \times 10^{+0}$	5.6647×10^{-1}	5.4868×10^{-2}	6.0390×10^{-3}	6.1588×10^{-4}
	3.22	3.36	3.18	3.29	
10^{-3}	31.7568	39.9892	0.89061	1.19691	1.75462
10^{-4}	7.56361	17.8442	80.8351	2.71873	2.79452
10^{-5}	2.29767	8.60822	28.5018	5.37233	5.2274
10^{-6}	15.3381	13.9091	15.5304	9.33243	1.08316

Table 2 Maximum absolute error E_ε^N, the rate of convergence p_ε^N and the uniform rate p^N for Example 1 by NSA on nonuniform mesh-I

ε	Number of mesh points N				
	16	32	64	128	256
10^{-2}	1.2490×10^{-3}	1.6421×10^{-4}	2.9018×10^{-5}	5.1319×10^{-6}	8.8588×10^{-7}
	2.92	2.50	2.49	2.53	
10^{-3}	6.2655×10^{-3}	5.3755×10^{-4}	5.5634×10^{-5}	7.8651×10^{-6}	1.2311×10^{-6}
	3.54	3.27	2.82	2.67	
10^{-4}	1.8304×10^{-2}	1.5213×10^{-3}	1.5098×10^{-4}	1.6462×10^{-5}	1.9913×10^{-6}
	3.58	3.33	3.19	3.04	
10^{-5}	4.0947×10^{-2}	3.3147×10^{-3}	3.2265×10^{-4}	3.5010×10^{-5}	4.0153×10^{-6}
	3.62	3.36	3.20	3.12	
10^{-6}	7.7800×10^{-2}	6.2211×10^{-3}	5.9198×10^{-4}	6.3639×10^{-5}	7.2872×10^{-6}
	3.64	3.39	3.21	3.12	
p^N	3.64	3.39	3.21	3.12	

Table 3 Maximum absolute error E_ε^N, the rate of convergence p_ε^N and the uniform rate p^N for Example 1 by NSA on nonuniform mesh-II

ε	Number of mesh points N				
	16	32	64	128	256
10^{-2}	1.8475×10^{-2}	1.2115×10^{-3}	1.0327×10^{-4}	9.9623×10^{-6}	1.0238×10^{-6}
	3.93	3.55	3.37	3.28	
10^{-3}	1.1261×10^{-1}	7.5501×10^{-3}	6.5023×10^{-4}	6.5497×10^{-5}	7.1369×10^{-6}
	3.89	3.53	3.31	3.19	
10^{-4}	2.8752×10^{-1}	2.1767×10^{-2}	1.8203×10^{-3}	1.8155×10^{-4}	1.9904×10^{-5}
	3.72	3.57	3.32	3.18	
10^{-5}	9.6631×10^{-1}	4.7176×10^{-2}	3.8466×10^{-3}	3.7546×10^{-4}	4.0886×10^{-5}
	4.35	3.61	3.35	3.19	
10^{-6}	5.0515	8.7328×10^{-2}	7.0498×10^{-3}	6.7170×10^{-4}	7.2359×10^{-5}
	5.85	3.63	3.39	3.21	
p^N	5.85	3.63	3.39	3.21	

Table 4 Maximum absolute error E_ε^N and the rate of convergence p_ε^N for Example 1 by the EFD scheme on uniform mesh

ε	Number of mesh points N				
	16	32	64	128	256
10^{-2}	9.8293×10^{-1}	4.6100×10^{-1}	1.5059×10^{-1}	3.5149×10^{-2}	7.6960×10^{-3}
	1.09	1.61	2.11	2.19	
10^{-3}	3.1510	2.4735	1.8109	1.1766	6.1063×10^{-1}
10^{-4}	5.4394	4.7478	4.0578	3.3710	2.6904
10^{-5}	7.7405	7.0475	6.3547	5.6622	4.9703
10^{-6}	10.043	9.3498	8.6567	7.9636	7.2706

meshes are shown in Table 5. We include in Table 6 the errors with the *BE* scheme on nonuniform mesh II. To apply these methods, the IVP must be linearized previously, which causes the poor performance of the schemes as it is shown in the numerical results.

Figure 1 corresponds to Example 1, where the exact solution and the numerical solution obtained by the NSA on nonuniform mesh-II are respectively denoted by the continuous line and dots for $\varepsilon = 10^{-2}$, 10^{-6} and $N = 32$.

Example 2 Consider the following nonlinear IVP which is a pseudo-second-order kinetic equation used to describe time evolution of adsorption under nonequilibrium conditions [11]

$$\begin{cases} \varepsilon\, u' = (1-u)^2, \quad x \in [0,1] \\ u(0) = 0.1 \end{cases}$$

Table 5 Maximum absolute error E_ε^N and the rate of convergence p_ε^N for Example 1 by the BE scheme on shishkin mesh

ε	Number of mesh points N				
	16	32	64	128	256
10^{-2}	3.8046×10^{-1}	2.0077×10^{-1}	1.0068×10^{-1}	4.8093×10^{-2}	2.2528×10^{-2}
	0.92	0.99	1.06	1.09	
10^{-3}	9.8503×10^{-1}	7.5469×10^{-1}	5.2322×10^{-1}	3.1369×10^{-1}	1.7109×10^{-1}
	0.38	0.53	0.74	0.87	
10^{-4}	1.4805	1.3085	1.1212	9.1813×10^{-1}	7.0269×10^{-1}
10^{-5}	1.8438	1.7168	1.5802	1.4318	1.2690
10^{-6}	2.1215	2.0228	1.9187	1.8077	1.6879

Table 6 Maximum absolute error E_ε^N, the rate of convergence p_ε^N and the uniform rate p^N for Example 1 by BE on nonuniform mesh-II

ε	Number of mesh points N				
	16	32	64	128	256
10^{-2}	3.1613×10^{-1}	1.3071×10^{-1}	4.3096×10^{-2}	3.0892×10^{-2}	2.9118×10^{-2}
	1.27	1.60	0.48	0.08	
10^{-3}	9.1319×10^{-1}	5.8224×10^{-1}	2.0837×10^{-1}	3.8359×10^{-2}	3.6669×10^{-2}
	0.65	1.48	2.44	0.06	
10^{-4}	1.4274	1.1702	7.5906×10^{-1}	1.5551×10^{-1}	3.8021×10^{-2}
	0.28	0.62	2.28	2.03	
10^{-5}	1.8043	1.6158	1.3120	6.5636×10^{-1}	3.8225×10^{-2}
	0.16	0.30	0.99	4.10	
10^{-6}	2.0906	1.9455	1.7193	1.2320	1.1069×10^{-1}
	0.10	0.17	0.48	3.47	
p^N	0.10	0.17	0.48	3.47	

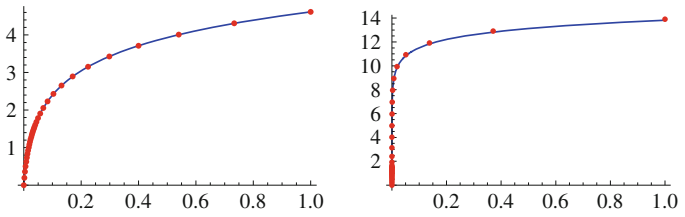

Fig. 1 Exact and numerical solutions for problem 1, $N = 32$ (*left* $\varepsilon = 10^{-2}$, *right* $\varepsilon = 10^{-6}$)

The exact solution of the IVP is given by

$$u(x) = \frac{9\,x + \varepsilon}{9\,x + 10\,\varepsilon}\,.$$

The maximum absolute errors for this example are presented in Tables 7 and 8 for different values of ε and N on Shishkin mesh and Nonuniform mesh-I (for Nonuniform mesh-II similar results are obtained). The errors given in these tables are constant and close to the machine precision. This is because the non-standard scheme integrates this IVP without local truncation error, and only error committed here is the round-off error. Because of this one cannot identify the convergence in Tables 7 and 8 when increasing N. We note that for the biggest value of N we obtain the big error due to the number of evaluations involved.

In Fig. 2, the exact solution (the continuous line) with the numerical solution (dots) of Example 2 obtained by the NSA on Shishkin mesh are plotted for $\varepsilon = 10^{-2},\ 10^{-6}$, and $N = 16$. We can observe the convergence to the fixed point of the differential equation $u(x) = 1$.

Example 3 Our next example is the IVP given by

$$\begin{cases} \varepsilon\, u' = \sin(u), & x \in [0, 1] \\ u(0) = u_0, \end{cases}$$

Table 7 Maximum absolute error E_ε^N for Example 2 by NSA on shishkin mesh

ε	Number of mesh points N				
	16	32	64	128	256
10^{-2}	1.1102×10^{-16}	2.2204×10^{-16}	2.2204×10^{-16}	3.3306×10^{-16}	4.4408×10^{-16}
10^{-3}	2.2204×10^{-16}	1.1102×10^{-16}	2.2204×10^{-16}	3.3306×10^{-16}	6.6613×10^{-16}
10^{-4}	3.8857×10^{-15}	4.4408×10^{-16}	1.6653×10^{-15}	7.3274×10^{-15}	8.8817×10^{-16}
10^{-5}	9.9253×10^{-14}	2.4758×10^{-14}	1.9795×10^{-13}	6.2172×10^{-15}	1.2323×10^{-14}
10^{-6}	2.0339×10^{-13}	7.0610×10^{-14}	1.5887×10^{-13}	1.2989×10^{-14}	8.7707×10^{-15}

Table 8 Maximum absolute error E_ε^N for Example 2 by NSA on nonuniform mesh-I

ε	Number of mesh points N				
	16	32	64	128	256
10^{-2}	2.2204×10^{-16}	2.2204×10^{-16}	2.2204×10^{-16}	2.2204×10^{-16}	3.3306×10^{-16}
10^{-3}	2.2204×10^{-16}	2.2204×10^{-16}	2.2204×10^{-16}	1.1102×10^{-16}	3.3306×10^{-16}
10^{-4}	6.0285×10^{-14}	8.2156×10^{-15}	1.7763×10^{-15}	2.2204×10^{-16}	2.2204×10^{-16}
10^{-5}	5.0504×10^{-13}	2.3869×10^{-13}	5.7731×10^{-14}	6.8833×10^{-15}	8.8817×10^{-16}
10^{-6}	9.8824×10^{-12}	1.6509×10^{-13}	7.2164×10^{-14}	4.5408×10^{-14}	7.2164×10^{-15}

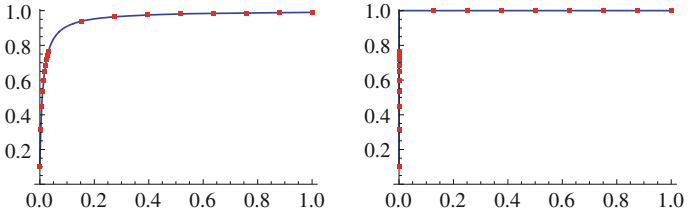

Fig. 2 Exact and numerical solutions for problem 2, $N = 16$ (*left* $\varepsilon = 10^{-2}$, *right* $\varepsilon = 10^{-6}$)

whose exact solution is

$$u(x) = 2\,\mathrm{arccot}\left(\exp\left(\frac{-x}{\varepsilon}\right)\cot\left(\frac{u_0}{2}\right)\right).$$

We take $u_0 \in (\pi/2, \pi)$ in order to assure the existence of a boundary layer at the initial point.

For this problem we have considered $u_0 = 2$ for the numerical tests. In this case it is $u'(x) > 0$ and the solution grows towards the fixed point $u(x) = \pi$.

For this problem, we have applied the non-standard algorithm (*NSA*) on uniform mesh, Nonuniform mesh-I and Nonuniform mesh-II. The maximum errors obtained on the uniform meshes are given in Table 9. Tables 10 and 11 respectively display the errors corresponding to Nonuniform mesh-I and Nonuniform mesh-II.

The plots of the exact solution (the continuous line) and the numerical solution (the dotted line) of Example 3 obtained by *NSA* on nonuniform mesh-II are shown in Fig. 3 for $\varepsilon = 10^{-2}$, 10^{-6}, and $N = 16$.

Example 4 Consider the following nonlinear IVP which models the kinetic behavior of biosorption [10, 23]:

$$\begin{cases} \varepsilon\, u' = u - u^3, & x \in (0, 1] \\ u(0) = 0.1\,. \end{cases}$$

Table 9 Maximum absolute error E_ε^N and the rate of convergence p_ε^N for Example 3 by NSA on uniform mesh

ε	Number of mesh points N				
	16	32	64	128	256
10^{-2}	$1.4787 \times 10^{+0}$	8.6413×10^{-1}	8.7951×10^{-2}	9.1077×10^{-3}	1.0053×10^{-3}
	0.77	3.29	3.327	3.17	
10^{-3}	1.5020	1.5020	1.5020	1.4983	1.1902
10^{-4}	1.5020	1.5020	1.5020	1.5020	1.5020
10^{-5}	1.5020	1.5020	1.5020	1.5020	1.5020
10^{-6}	1.5020	1.5020	1.5020	1.5020	1.5020

Table 10 Maximum absolute error E_ε^N, the rate of convergence p_ε^N and the uniform rate p^N for Example 3 by NSA on nonuniform mesh-I

ε	Number of mesh points N				
	16	32	64	128	256
10^{-2}	5.0604×10^{-3}	6.0776×10^{-4}	7.4404×10^{-5}	9.4527×10^{-6}	1.2208×10^{-6}
	3.05	3.03	2.97	2.95	
10^{-3}	1.6167×10^{-2}	1.8496×10^{-3}	2.2471×10^{-4}	2.8202×10^{-5}	3.6339×10^{-6}
	3.12	3.04	2.99	2.95	
10^{-4}	1.6090×10^{-2}	3.6832×10^{-3}	4.7714×10^{-4}	6.0029×10^{-5}	7.6669×10^{-6}
	2.12	2.94	2.99	2.96	
10^{-5}	5.7491×10^{-2}	7.2491×10^{-3}	8.8257×10^{-4}	1.0770×10^{-4}	1.3749×10^{-5}
	2.98	3.03	3.03	2.96	
10^{-6}	6.6146×10^{-2}	1.2005×10^{-2}	1.4597×10^{-3}	1.7660×10^{-4}	2.2172×10^{-5}
	2.46	3.03	3.04	2.99	
p^N	2.46	3.03	3.04	2.99	

Table 11 Maximum absolute error E_ε^N, the rate of convergence p_ε^N and the uniform rate p^N for Example 3 by NSA on nonuniform mesh-II

ε	Number of mesh points N				
	16	32	64	128	256
10^{-2}	1.3753×10^{-3}	7.0224×10^{-5}	1.5086×10^{-5}	2.9757×10^{-6}	5.5314×10^{-7}
	4.29	2.21	2.34	2.42	
10^{-3}	3.0045×10^{-3}	9.4651×10^{-5}	1.5086×10^{-5}	2.9757×10^{-6}	5.5314×10^{-7}
	4.98	2.64	2.34	2.42	
10^{-4}	4.3323×10^{-3}	1.7782×10^{-4}	1.5086×10^{-5}	2.9757×10^{-6}	5.5314×10^{-7}
	4.60	3.55	2.34	2.42	
10^{-5}	1.0100×10^{-2}	3.0562×10^{-4}	1.5086×10^{-5}	2.9757×10^{-6}	5.5314×10^{-7}
	5.04	4.34	2.34	2.42	
10^{-6}	1.9356×10^{-2}	5.9321×10^{-4}	1.5086×10^{-5}	2.9757×10^{-6}	5.5314×10^{-7}
	5.02	5.29	2.34	2.42	
p^N	5.02	5.29	2.34	2.42	

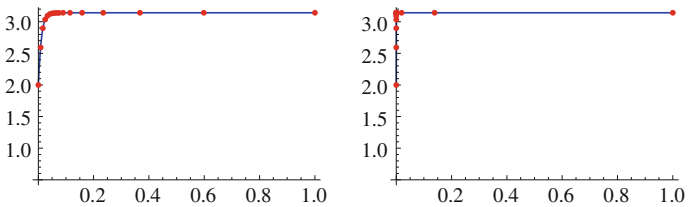

Fig. 3 Exact and numerical solutions for problem 3, $N = 16$ (*left* $\varepsilon = 10^{-2}$, *right* $\varepsilon = 10^{-6}$)

The exact solution of this IVP is

$$u(x) = \frac{\exp\left(\frac{x}{\varepsilon}\right)}{\sqrt{99 + \exp\left(\frac{2x}{\varepsilon}\right)}}.$$

The maximum pointwise error of Example 4 obtained from the *NSA* on uniform mesh are given in Table 12, which shows that the non-standard algorithm is not working for smaller values of the parameter ε on uniform mesh. Table 13 and Table 14 correspond to Example 4 for NSA on nonuniform mesh-I and II respectively. The maximum pointwise errors of Tables 13 and 14 reveal the necessity of nonuniform

Table 12 Maximum absolute error E_ε^N and the rate of convergence p_ε^N for Example 4 by NSA on uniform mesh

ε	Number of mesh points N				
	16	32	64	128	256
10^{-2}	$2.2565 \times 10^{+0}$	5.4571×10^{-1}	4.8587×10^{-2}	7.0421×10^{-3}	9.1136×10^{-4}
	2.04	3.48	2.78	2.94	
10^{-3}	2.43236	2.43236	19.0733	2.3956	1.1604
10^{-4}	5.3859	2.4323	104.3440	54.3092	2.4323
10^{-5}	3.1067	2.7225	2.5681	2.4323	2.4323
10^{-6}	2.4323	5.4045	5.8562	12.6773	2.4323

Table 13 Maximum absolute error E_ε^N, the rate of convergence p_ε^N and the uniform rate p^N for Example 4 by NSA on nonuniform mesh-I

ε	Number of mesh points N				
	16	32	64	128	256
10^{-2}	6.8430×10^{-3}	8.9378×10^{-4}	1.1244×10^{-4}	1.4552×10^{-5}	1.9191×10^{-6}
	2.93	2.99	2.94	2.92	
10^{-3}	2.1844×10^{-2}	2.6760×10^{-3}	3.1198×10^{-4}	4.0469×10^{-5}	5.2240×10^{-6}
	3.02	3.10	2.94	2.95	
10^{-4}	2.0041×10^{-2}	5.7444×10^{-3}	6.6968×10^{-4}	8.2918×10^{-5}	1.0669×10^{-5}
	1.80	3.10	3.01	2.95	
10^{-5}	9.6759×10^{-2}	1.1142×10^{-2}	1.0938×10^{-3}	1.4799×10^{-4}	1.8795×10^{-5}
	3.11	3.34	2.88	2.97	
10^{-6}	1.1199×10^{-1}	1.3880×10^{-2}	1.8867×10^{-3}	2.4068×10^{-4}	2.9800×10^{-5}
	3.01	2.87	2.97	3.01	
p^N	3.01	2.87	2.97	3.01	

Table 14 Maximum absolute error E_ε^N, the rate of convergence p_ε^N and the uniform rate p^N for Example 4 by NSA on nonuniform mesh-II

ε	Number of mesh points N				
	16	32	64	128	256
10^{-2}	5.4840×10^{-4}	8.2133×10^{-5}	1.7949×10^{-5}	3.5867×10^{-6}	6.7191×10^{-7}
	2.73	2.19	2.32	2.41	
10^{-3}	1.1760×10^{-3}	8.2133×10^{-5}	1.7949×10^{-5}	3.5867×10^{-6}	6.7191×10^{-7}
	3.83	2.19	2.32	2.41	
10^{-4}	2.3775×10^{-3}	8.2133×10^{-5}	1.7949×10^{-5}	3.5867×10^{-6}	6.7191×10^{-7}
	4.85	2.19	2.32	2.41	
10^{-5}	3.9704×10^{-3}	8.2133×10^{-5}	1.7949×10^{-5}	3.5867×10^{-6}	6.7191×10^{-7}
	5.59	2.19	2.32	2.41	
10^{-6}	5.3368×10^{-3}	8.2133×10^{-5}	1.7949×10^{-5}	3.5867×10^{-6}	6.7191×10^{-7}
	6.02	2.19	2.32	2.41	
p^N	6.02	2.19	2.32	2.41	

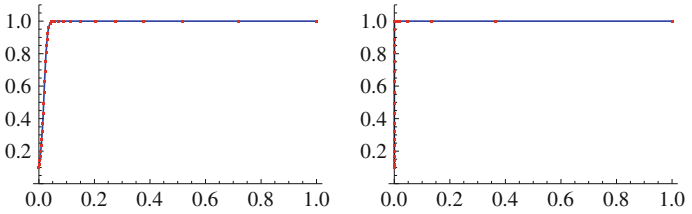

Fig. 4 Exact and numerical solutions for problem 4, $N = 32$ (*left* $\varepsilon = 10^{-2}$, *right* $\varepsilon = 10^{-6}$)

mesh for singularly perturbed IVPs. Table 14 shows the third-order uniformly convergent behavior.

In Fig. 4, we plotted the exact solutions (in continuous line) and the numerical solution (in dotted line) obtained by the *NSA* on the Nonuniform mesh-II for $\varepsilon = 10^{-2}$, 10^{-6} and $N = 32$.

6 Conclusions

In this article, we have presented a numerical method for singularly perturbed nonlinear autonomous IVPs. The solution of these problems has a multiscale character, and one has to use special nonuniform meshes to solve these problems. If one wants to apply the existing techniques in the literature, then the nonlinear IVP has to be linearized firstly. One may loose so many nice properties of the solution by linearizing the problem. But there is no linearization is required for the present method. To capture the fastly varying solution inside the initial layer, we are using some nonuniform meshes. The numerical results presented in the previous section reveal this fact.

Acknowledgments The authors wish to thank JCYL project SA050A08 and MICYT project MTM2008/05489 for financial support.

References

1. R. Aris, On stability criteria of chemical reaction engineering. Chem. Eng. Sci. **24**, 149–169 (1968)
2. W. Benzinger, A. Becker, K.J. Hüttinger, Chemistry and kinetics of chemical vapour deposition of pyrocarbon: I. Fundamentals of kinetics and chemical reaction engineering. Carbon **34**, 957–966 (1996)
3. A. Burghardt, T. Zaleski, Longitudinal dispersion at small and large Peclet numbers in chemical flow reactors. Chem. Eng. Sci. **23**, 575–591 (1968)
4. D.S. Cohen, Multiple stable solutions of nonlinear boundary value problems arising in chemical reactor theory. SIAM. J. Appl. Math. **20**(1), 1–13 (1971)
5. D.S. Cohen, T.W. Laetsch, Nonlinear boundary value problems suggested by chemical reactor theory. J. Differ. Equ. **7**, 217–226 (1970)
6. M. Danish, R.K. Sharma, S. Ali, Gas absorption with first order chemical reaction in a laminar falling film over a reacting solid wall. Appl. Math. Model. **32**, 901–929 (2008)
7. E.P. Doolan, J.J.H. Miller, W.H.A. Schildres, *Uniform Numerical Methods for Problems with Initial and Boundary Layers* (Boole Press, Dublin, 1980)
8. P.A. Farrell, Uniform and optimal schemes for stiff initial-value problems. Comput. Math. Appl. **13**, 925–936 (1987)
9. M.K. Jain, *Numerical Solution of Differential Equations* (Wiley Eastern Limited, New Delhi, 1984)
10. Y. Liu, L. Shen, A general rate law equation for biosorption. Biochem. Eng. J. **38**, 390–394 (2008)
11. Y. Liu, New insights into pseudo-second-order kinetic equation for adsorption. Colloids Surf. A **320**, 275–278 (2008)
12. R. Lovas, P. Kacsuk, I. Lagzi, T. Turányi, Unified development solution for cluster and grid computing and its application in chemistry. Lect. Notes Comput. Sci. **3044**, 226–235 (2004)
13. J.J.H. Miller, Optimal uniform difference schemes for linear initial-value problems. Comput. Math. Appl. **12**, 1209–1215 (1986)
14. J.J.H. Miller, E. O'Riordan, G.I. Shishkin, *Fitted Numerical Methods for Singular Perturbation Problems* (World Scientific, Singapore, 1996)
15. S. Natesan, N. Ramanujam, Initial-value technique for singularly perturbed boundary-value problems for second-order ordinary differential equations arising in chemical reactor theory. J. Optim. Theory Appl. **97**(2), 455–470 (1998)
16. S. Natesan, N. Ramanujam, A booster method for singular perturbation problems arising in chemical reactor theory. Appl. Math. Comput. **100**, 27–48 (1999)
17. S. Natesan, J. Vigo-Aguiar, N. Ramanujam, A numerical algorithm for singular perturbation problems exhibiting weak boundary layers. Comput. Maths. Appl. **45**, 469–479 (2003)
18. R.E. O'Malley, *Introduction to Singular Perturbation* (Academic Press, New York, 1974)
19. H. Ramos, A non-standard explicit integration scheme for initial-value problems. Appl. Math. Comput. **189**, 710–718 (2007)
20. H. Ramos, J. Vigo-Aguiar, A new algorithm appropriate for solving singular and singularly perturbed autonomous initial-value problems. Int. J. Comput. Math. **85**, 603–611 (2008)
21. C.V. Rao, D.M. Wolf, A.P. Arkin, Control, exploitation and tolerance of intracellular noise. Nature **420**, 231–237 (2002)
22. M.J.O Reilly, E. O'Riordan, A Shishkin mesh for a singularly perturbed riccati equation. J. Comput. Appl. Math. **182**, 372–387 (2005)
23. W. Rudzinski, W. Plazinski, Kinetics of solute adsorption at solid/solution interfaces: a theoretical development of the empirical pseudo-first and pseudo-second order kinetic rate equations, based on applying the statistical rate theory of interfacial transport. J. Phys. Chem. B **110**, 16514–16525 (2006)
24. J. Vigo-Aguiar, S. Natesan, A parallel boundary value technique for singularly perturbed two-point boundary value problems. J. Supercomput. **27**, 195–206 (2004)